Rheology of crossbridge ensembles

Khoi D. Nguyen[1] and Madhusudhan Venkadesan[1]

[1]*Department of Mechanical Engineering & Materials Science, Yale University, New Haven, CT, USA*

December 29, 2021

Abstract

Muscle rheology, or the characterization of a muscle's response to external mechanical perturbations, is crucial to an animal's motor control and locomotive abilities. How the rheology emerges from the ensemble dynamics of microscopic actomyosin crossbridges known to underlie muscle forces is however a longstanding question. Classical descriptions in terms of force-length and force-velocity relationships capture only part of the rheology, namely under steady but not dynamical conditions. Although much is known about the actomyosin machinery, current mathematical models that describe the behavior of a population or an ensemble of crossbridges are plagued by an excess of parameters and computational complexity that limits their usage in large-scale musculoskeletal simulations. In this paper, we examine models of crossbridge dynamics of varying complexity and show that the emergent rheology of an ensemble of crossbridges can be simplified to a few dominant time-constants associated with intrinsic dynamical processes. For Huxley's classical two-state crossbridge model, we derive exact analytical expressions for the emergent ensemble rheology and find that it is characterized by a single time-constant. For more complex models with up to five crossbridge states, we show that at most three time-constants are needed to capture the ensemble rheology. Our results thus yield simplified models comprising of a few time-constants for muscle's bulk rheological response that can be readily used in large-scale simulations without sacrificing the model's interpretability in terms of the underlying actomyosin crossbridge dynamics.

Introduction

Muscle exerts force in response to neural inputs and external pertubations of its length (Nishikawa et al., 2018; Zajac, 1989). Like most soft passive materials, the length perturbation-induced forces, or simply perturbation response, relaxes over time (Huxley and Simmons, 1971; Nguyen et al., 2018) and the timescales involved are crucial for the functional role of muscle because they enable faster-than-reflex reactions (Bizzi et al., 1982; Hogan et al., 1987; Nishikawa et al., 2007; Nguyen et al., 2018, figure 1a). For example, on durations shorter than the relaxation timescales, the perturbation response is nearly unchanging and the muscle functions as an elastic solid body that resists stretching and help elastic energy storage in

tendons (Bizzi et al., 1982; Biewener and Roberts, 2000). And on durations longer, the perturbation response relaxes significantly and a muscle functions like a viscous damper which enables rapid postural changes and kinetic energy dissipation (Lin and Rymer, 2000; Konow et al., 2012). But unlike passive materials, a muscle's relaxation timescales are neurally regulated by active molecular interactions of myosin motors with actin filaments (Huxley and Tideswell, 1996), and whether a muscle functions like an elastic body or a viscous damper is subject to neural control. Thus, formulating a muscle's perturbation response in terms of its underlying molecular machinery helps to identify the interplay of neural inputs and rheology in an animal's motor control of its muscles (Nguyen et al., 2018; Bizzi et al., 1982; Nishikawa et al., 2018, figure 1a).

Muscle properties such as short-range stiffness, viscous damping, loss modulus, and storage modulus are examples of bulk rheological properties (Rack and Westbury, 1974; Konow et al., 2012; Kawai and Brandt, 1980) that are characterizations of the muscle's perturbation response and are analogous to similar characterizations of passive materials (Tschoegl, 2012) and active materials (Gardel et al., 2004; Koenderink et al., 2009). In muscle, these bulk rheological properties arise from contributions of muscle's passive tissues, geometry, and internal molecular machinery (Sleboda and Roberts, 2020; Fung, 2013). The mapping from the microscopic dynamics of the molecular machinery to its contributions to bulk properties remains incomplete, however, and this gap is exemplified by the split between two classes of widely used muscle models. Namely, macroscopic phenomenological models and microscopic mechanochemical models that idealize muscles as one-dimensional structures.

Phenomenological models inspired by A.V. Hill's work (Hill, 1938) are widely used to quantitatively describe muscle's force production capabilities (Zajac, 1989; MacIntosh and MacNaughton, 2005; Fung, 1971; Todorov, 2003). These models incorporate an active contractile element, a parallel element that is often modeled as a passive elastic or viscoelastic material, and a series elasticity that captures tendon and other passive tissue compliance [figure 1b]. The passive parallel element represents non-contractile tissues and the intramuscular fluid that have well-known effects on the contractile force capacity of muscle (Sleboda and Roberts, 2020). But muscle's perturbation response is dominated by the active contractile element except under extreme eccentric conditions where the passive parallel element is important (MacIntosh and MacNaughton, 2005; Lindstedt et al., 2001). In Hill-type models, the perturbation response of the active element are represented by isometric force-length and isotonic force-velocity properties and its interactions with the series elasticity (Zajac, 1989; Todorov, 2003), but these properties are known to lose predictive value during locomotive situations where non-isometric and non-isotonic conditions that lead to transient and non-steady perturbation responses are commonplace (Lee et al., 2013; Sandercock and Heckman, 1997; Dick et al., 2017; Rice et al., 2020; Perreault et al., 2003, figure 1b). Furthermore, parameters in phenomenological models do not lend themselves to interpretation in terms of known mechanochemical processes within muscle. Despite these shortcomings, phenomenological models remain the most viable means to perform large-scale biomechanical simulations and optimal control calculations because of their low computational burden and ease of implementation (De Groote and Falisse, 2021; O'Neill et al., 2013; Miller, 2014).

The flip side to phenomenological models are those that incorporate the current state of understanding of the microscopic mechanochemical cycles that drive muscle. The hydrolysis of ATP by myosin motors during formation of actin-myosin crossbridges underlie active mus-

cle contraction and perturbation response (Lymn and Taylor, 1971; Holmes, 1997; Huxley and Simmons, 1971). Each myosin undergoes the biochemical Lymn-Taylor cycle in which it attaches to and detaches from actin filaments based on ATP capture, hydrolysis, and release of byproducts (Lymn and Taylor, 1971). There are different modeling approximations of this cycle that incorporate different numbers of intermediate states [figure 1b]. The biochemical Lymn-Taylor cycle is coupled to a mechanical cycle that converts chemical energy to mechanical work. When attached, each myosin motor pulls on the actin filament to generate piconewton forces and around 10 nm power strokes. The collective action of many motors is modeled as an ensemble of stochastically cycling crossbridges whose force contributions add up (Huxley, 1957; Huxley and Simmons, 1971). Mechanical perturbation of the whole muscle ultimately perturbs the mechanochemical crossbridge cycle whose dynamics are load and strain-dependent (Palmer, 2010; Liu et al., 2018), which in turn alters the force produced by the ensemble and, in principle, manifests as bulk rheological properties of muscle. But crossbridge models employ numerous biochemical parameters that cannot be directly measured because of which we lack a mechanistic understanding of muscle's emergent rheology. This is the so called scale-connection problem.

Addressing the scale-connection problem would overcome many of the shortcomings of both microscopic and macroscopic models, and is a major objective of neuromuscular research (Nishikawa et al., 2018). The distribution-moment formalism was a crucial step in on-going efforts to address it and presented a general approach to simplifying microscopic models without relying on the exact choice of how a crossbridge cycle is modeled (Zahalak, 1981, 1986; Zahalak and Ma, 1990). Specifically, the formalism assumed a Gaussian distribution for the fraction of bound crossbridges as a function of crossbridge strain such that the governing ensemble dynamics is approximated by the dynamics of measurable macroscopic quantities: stiffness, forces, and elastic energy storage. Thus, it is an approximate yet tractable mapping from these macroscopic quantities to the ensemble dynamics. But in assuming a preset distribution and not one that emerges from the crossbridge dynamics, it stops short of connecting scales back to the crossbridge cycle. Shortcomings of this approximation are evident from multiple perturbation experiments which show that the distribution-moment model does not accurately capture muscle forces, but more complex crossbridge models may be able to do so by sacrificing computational speed (Cole et al., 1996; van den Bogert et al., 1998). So a gap remains in mapping crossbridge theory to the emergent rheology of its ensemble.

In this paper, we connect the dynamics of a single crossbridge to the rheology of an ensemble or population of crossbridges that represents a whole sarcomere. In particular, we analyze the ensemble behavior of several different crossbridge models to identify a minimal parameter-set that affects their emergent rheology. The paper begins with a brief tutorial on rheological characterization of materials using complex modulus and dynamic stiffness. Then we use numerical simulations of large ensembles of crossbridges, ranging in complexity from two-state to five-state crossbridge models, to identify commonalities and differences in their perturbation responses. Next we analytically derive the rheology of a two-state crossbridge model and show how a single exponential relaxation process with one time-constant suffices to capture its rheology, how that relaxation is related to the crossbridge dynamics, and provide a mechanical interpretation in terms of elastic and viscous material properties. We then extend the characterization to more complex crossbridge models by adding multiple exponential

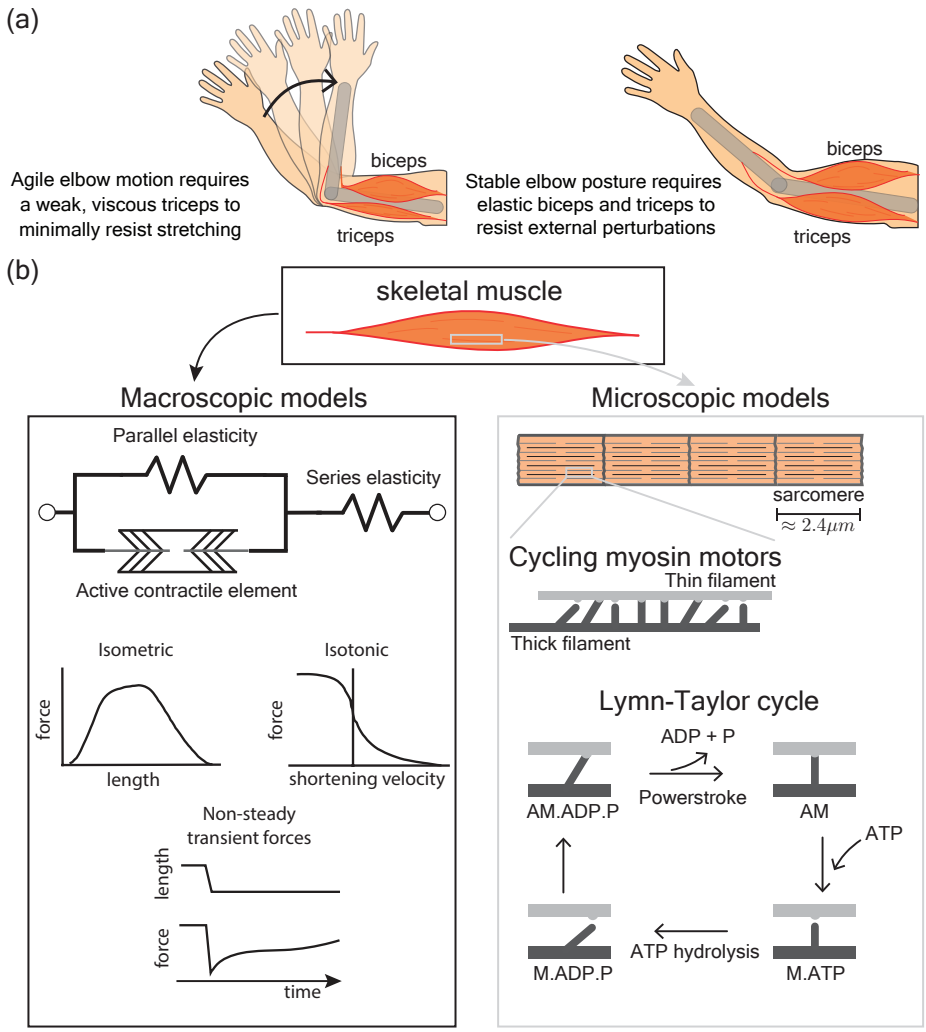

Figure 1: Current models of skeletal muscles. (a) An example of the motor functionalities provided by a muscle's rheological response to perturbations. (b) Widely used muscle models can be separated into microscopic biochemical models and macroscopic phenomenological models. The microscopic models track the dynamics of myosin motors whereas macroscopic models apply isometric and isometric characterizations and transient forces to capture the active contractile element. The isometric and isotonic characterizations are adapted from figure 8 of Zajac 1989 and the transient forces are adapted from figure 3 of Huxley and Simmons 1971. The current paper seeks to connect the crossbridge cycle dynamics to the emergent generalized transient force response beyond the isometric and isotonic characterizations of muscle.

processes and discuss the implications of our work to the development of computationally efficient and parametrically parsimonious models that are still interpretable in terms of the microscopic mechanochemical dynamics of actomyosin crossbridges.

Preliminaries

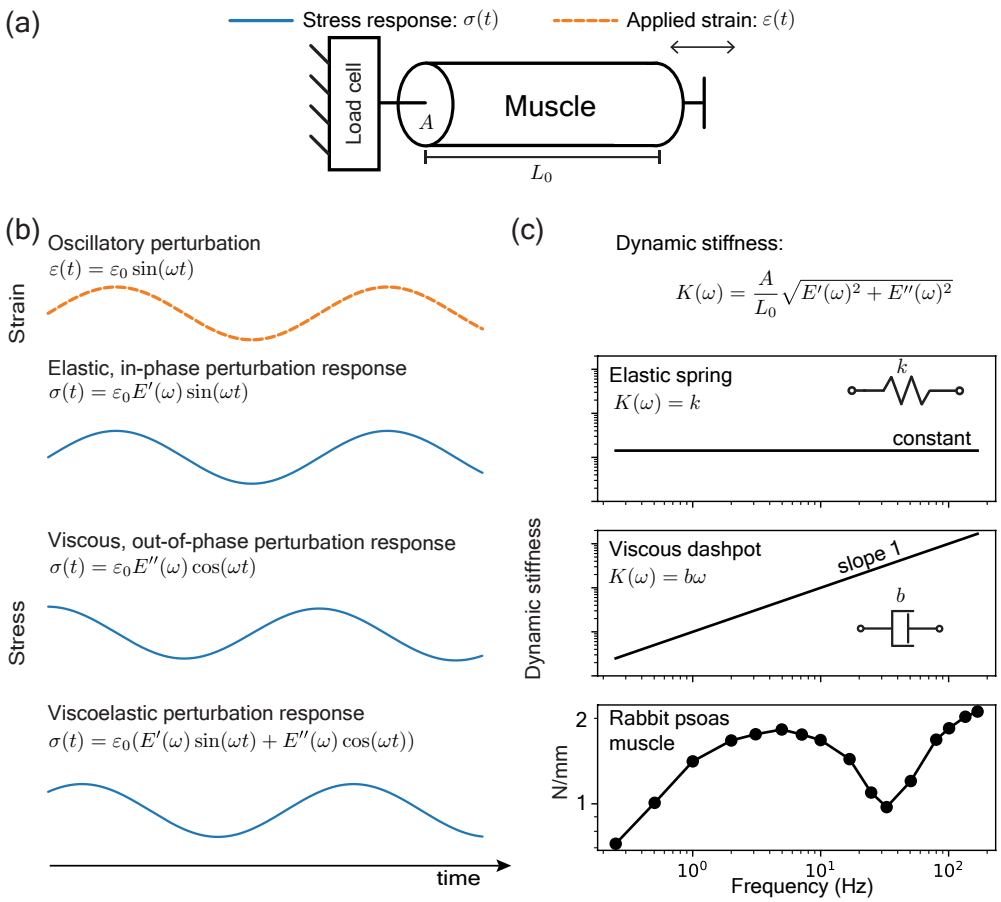

Figure 2: Linear rheological characterization of muscles. (a) Schematic of an experimental setup to measure a muscle's response to perturbations. (b) For an oscillatory length perturbation, the linear rheological response is characterized by an elastic modulus $E'(\omega)$ that measures the in-phase response and a loss modulus $E''(\omega)$ that measures the out-of-phase response. A general viscoelastic response has both in-phase and out-of-phase components. (c) The dynamic stiffness $K(\omega)$ is a third oscillatory rheological characterization. It is constant if the muscle is elastic and linearly proportional to frequency if the muscle is viscous. The dynamic stiffness of a rabbit psoas muscle is viscoelastic with features more complicated than elastic springs and viscous dashpots alone. The rabbit psoas plot is adapted from figure 3 of Kawai and Brandt 1980.

We focus here on the linear rheological characterization of muscle, which has proven useful in developing predictive models of muscle behavior (Rack and Westbury, 1974; Nguyen et al., 2018; Bizzi et al., 1982) and in interpreting *in vivo* muscle function for both large and small perturbations (Palmer et al., 2020; Niederer et al., 2019). A central quantity in linear rheology is the material modulus defined as the ratio of the measured stress to the applied strain. The modulus for muscle depends on the rate at which the strain is applied and varies over time. Using the Laplace or Fourier transform (Ogata, 2004), the applied

strain and the resulting stress response can each be decomposed into a sum of sinusoids of different temporal frequencies, and their ratio yields a frequency-dependent modulus. This characterization, a core tool in oscillatory rheology (Weitz et al., 2007; Tschoegl, 2012), provides an interpretation of muscle material properties in terms of frequency-dependent loss, storage, and complex moduli (Kawai and Brandt, 1980; Nguyen et al., 2018; Nguyen and Venkadesan, 2021). If the applied strain is a small-amplitude sinusoidal wave, then the resulting stress is approximately sinusoidal with both in-phase and out-of-phase components with respect to the applied strain [figure 2(a-b)]. The amplitude of the in-phase stress and out-of-phase stress divided by the applied strain amplitude define the storage modulus $E'(\omega)$ and loss modulus $E''(\omega)$, respectively. These moduli are a function of the oscillatory frequency ω. The complex modulus $E^*(\omega) = E'(\omega) + iE''(\omega)$ is a compact representation of the spring-like storage modulus and damper-like loss modulus. The dynamic stiffness $K(\omega)$ of sinusoidal analysis is related to the complex modulus as $K(\omega) = (A/L_0)|E^*(\omega)|$ for a muscle tissue of cross-sectional area A and length L_0. If muscle were elastic like a Hookean spring, then $K(\omega)$ is a constant independent of frequency. If muscle were viscous like a Newtonian fluid, then $K(\omega)$ is linearly proportional to frequency. In reality, muscle is neither extreme and exhibits intermediate viscoelastic behavior [figure 2c].

Results

Numerical simulations of ensemble crossbridge models

We numerically compute the emergent rheology of an ensemble or population of independently cycling crossbridges using previously published crossbridge models. The aim here is to survey the literature and use models that differ in complexity and in the types of muscle phenomena that each were originally designed to capture. To that end, we implement four crossbridge models ranging from two to five internal states (Huxley, 1957; Murase et al., 1986; Smith, 1998; Lombardi and Piazzesi, 1990). Importantly, our selection of crossbridge models is a representative but not exhaustive survey of all muscle phenomena under active research (Campbell, 2009; Stewart et al., 2010; McNamara et al., 2015; Nishikawa et al., 2018; Walcott, 2014; Williams et al., 2012). For example, the super relaxed myosin state introduces a new detached state with orders of magnitude lower ATP turnover than the normal detached state (Stewart et al., 2010; McNamara et al., 2015). Thin filament activation and cooperative mechanisms can introduce a coupling between crossbridges that break the assumption of independently cycling crossbridges (Walcott, 2014). Spatially explicit sarcomere models account for the distribution of crossbridges within the sarcomere and thus also for position-dependent crossbridge dynamics (Daniel et al., 1998; Williams et al., 2012). Although the crossbridge literature is broader than our selection, and likely any similarly sized selection, can reasonably sample, our objective with numerical simulations is to connect the emergent ensemble rheology with the detailed modeling choices regardless of the specific crossbridge model.

The simplest of the crossbridge models considered is Huxley's original two-state formulation that helped set the foundation for the whole class of crossbridge models developed since and its emergent rheology can thus serve as a point of reference (Huxley, 1957). In it,

Huxley idealizes crossbridges as molecular springs that stochastically attach to and detach from a rigid thick and thin filament backbone. The total elastic resistance of a population of these crossbridges is then taken to characterize the active and transient forces of muscles and, in turn, also the rheology of muscles. The other more complex crossbridge models refine Huxley's formation by incorporating additional attached and detached states which allows for new and higher-order dynamics that Huxley's two-state model may not capture. The three-state model by Murase et al., 1986 (Murase et al., 1986) showed that a second attached internal state is necessary to capture the three dominant sinusoidal processes observed in insect flight muscles. The four-state model by Smith, 1998 (Smith, 1998) proposed a minimal kinetic scheme to capture the force transients resulting from the phosphate release and ATP capture of the Lymn-Taylor cycle (Lindstedt et al., 2001). And lastly, the five-state model of Lombardi and Piazzesi, 1990 (Lombardi and Piazzesi, 1990) proposed a relatively complex kinetic scheme to capture the force transients of a frog skeletal muscle fiber under steady lengthening that, notedly, incorporated a forced detached state accessible only when crossbridges are stretched beyond a critical distance. The numbers of parameters involved for each model are many with 4 for Huxley's two-state model, 16 for the three-state model, 17 for the four-state model, and 24 for the five-state model. These parameters define the neutral length, stiffness of each attached crossbridge state, and the strain-dependent transition rates between them. A natural question that arises is how the emergent ensemble rheology depends on these parameters and, given such a vast parameter space, whether there is parameter-reduction that recapitulates the emergent rheology. We shall explore if such a parameter reduction is possible in the numerical simulations below.

The emergent ensemble rheologies of the selected crossbridge models are computed in terms of the dynamic stiffness, the variation of which with frequency determines whether the ensemble is like an elastic solid or a viscous damper. Numerically, we integrate each model's governing differential equations to compute the force response of an ensemble of crossbridges to a step length perturbation. The ensemble is initially at steady-state equilibrium so the emergent rheology arises from the ensemble's relaxation back to steady-state. Transforming the computed force response and the imposed step length perturbation into the frequency domain and taking their ratio directly yields the dynamic stiffness [Methods A].

We find that a simple behavior emerges at high and low frequencies regardless of model complexity and that the difference between crossbridge models manifest only on intermediate frequencies [figure 3b]. Specifically, the dynamic stiffness is constant at high frequencies and linearly proportional to ω at low frequencies, i.e. the dynamic stiffness is approximately

$$K(\omega) \approx \begin{cases} k & \text{for high frequencies,} \\ b \cdot \omega & \text{for low frequencies.} \end{cases} \tag{1}$$

These asymptotic regimes imply that the ensemble is an elastic solid with spring constant k at high frequencies and a viscous damper with damping coefficient b at low frequencies. But the dynamic stiffness at intermediate frequencies is more complicated in their frequency dependence, differs between the model variants, and does not immediately present a mechanical interpretation. We calculate a bandwidth in this intermediate frequency range where the dynamic stiffness differs by more than 5% from the asymptotic response [grey bars in inset of figure 3b] as a measure of complexity in the emergent rheology and is a measure

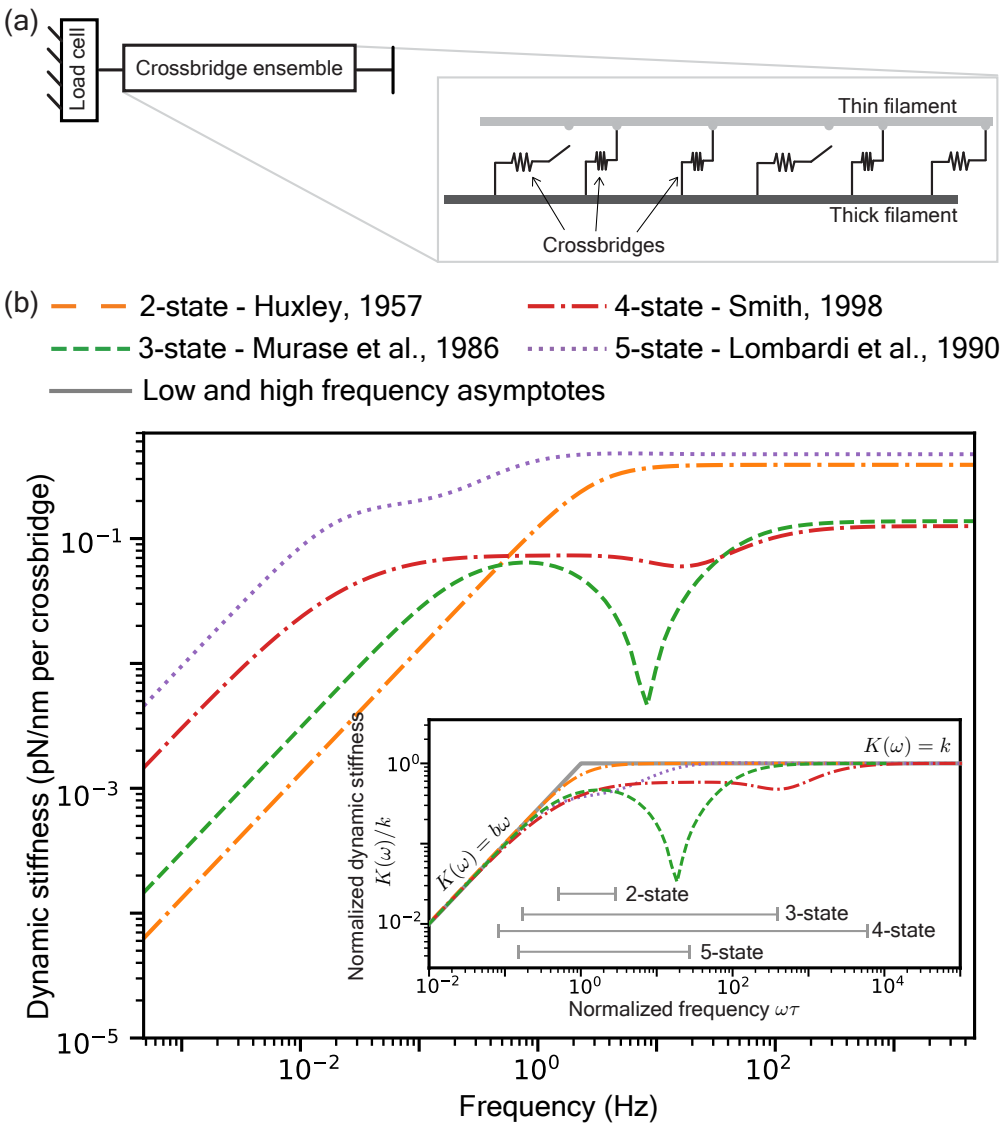

Figure 3: Rheology of the ensemble dynamics of different crossbridge models. (a) An ensemble of crossbridges operate collectively to model muscle forces. (b) The frequency-dependent dynamic stiffness of different crossbridge models resembles an elastic spring at high frequencies and a viscous dashpot at low frequencies. (inset) Collapse of different models onto equation (1) by normalizing the axes. For each model, the dynamic stiffness is normalized by the value k computed at the highest frequency. The frequency axis is normalized by a time-constant τ at which the two asymptotic behaviors match. The gray bars indicate the bandwidth over which the models deviate by more than 5% from their asymptotic behavior s.

distinct from the number of internal states used. The bandwidth is also indicative of computational cost because the largest time-step that can be used for numerical integration is governed by the high-frequency end of the bandwidth whereas the duration of time needed for the transient response to settle down is governed by the low-frequency end. We find that

the two-state Huxley model has the smallest bandwidth and is followed by the five-state, three-state, and four-state models. This ordering does not follow the number of internal states so the complexity of the emergent rheology does not correlate with complexity of the crossbridge model. For example, although the five-state model requires 24 parameters, the largest amongst all models considered, its emergent rheology is well-approximated as a high-frequency elastic spring and a low-frequency vicious damper which requires only two parameters and suggests that a drastic parameter reduction from the detailed crossbridge model to its emergent rheology is possible. We shall analyze the mathematical forms of these crossbridge models to derive the exact form of the parameter reduction.

Rheology of the generalized two-state crossbridge model

We analytically derive the rheology for the two-state crossbridge ensemble to examine the rheological features at intermediate frequencies that are not captured by the high and low frequency asymptotes [equation (1)]. We refer to (Smith, 1998) for a conceptually identical but more general derivation of a four-state crossbridge model while we focus here on the simpler two-state variant to demonstrate how modeling choices lead to different rheological features.

Two-state crossbridges cycle between making and breaking bonds between rigid thick and thin filaments. The attachment rate $f(x)$ and detachment rate $g(x)$, to form and break bonds, respectively, are functions of the distance x between the location of the myosin motor on the thick filament and the nearest binding site on the thin filament. At every distance x and time t, the proportion of attached crossbridges is $n(x,t)$, also known as the bond distribution, and the detached proportion is $(1-n(x,t))$. The bond distribution $n(x,t)$ evolves in time according to

$$\frac{dn(x,t)}{dt} = (1-n(x,t))f(x) - n(x,t)g(x). \tag{2}$$

This first-order differential equation has a steady-state bond distribution $n_{\text{ss}}(x) = f(x)/(f(x)+g(x))$ at equilibrium. Starting with this equilibrium bond distribution, a step length perturbation of amplitude a is delivered at $t=0$ to elongate the whole system and held there. Every crossbridge that was a distance x away from its nearest binding site is now a distance $(x+a)$ away and the distribution of crossbridges $n(x,t)$ evolves in time to relax back to its equilibrium state according to equation (2). The response to this step length perturbation is obtained using $n(x,0) = n_{\text{ss}}(x-a)$ as the initial condition and integrating equation (2) to find

$$n(x,t) = n_{\text{ss}}(x) + (n_{\text{ss}}(x-a) - n_{\text{ss}}(x))e^{-t(f(x)+g(x))}. \tag{3}$$

Therefore, $n(x,t)$ exponentially relaxes to its steady-state $n_{\text{ss}}(x)$ at a rate $f(x)+g(x)$. We illustrate this relaxation process in figure 4a using Huxley's rate functions (Huxley, 1957). The force $\Delta F(t)$ in response to the step length perturbation is determined by the difference between $n(x,t)$ and its steady state $n_{\text{ss}}(x)$. In terms of crossbridge stiffness λ_{xb} in units of [force/length] and crossbridge density M in units of [length]$^{-1}$, the force response is,

$$\Delta F(t) = M\lambda_{\text{xb}} \int_{-\infty}^{\infty} x(n_{\text{ss}}(x-a) - n_{\text{ss}}(x))e^{-t(f(x)+g(x))}dx. \tag{4}$$

By restricting our attention to the linear regime, *i.e.* a small perturbation a, the force response simplifies to

$$\Delta F(t) = -Ma\lambda_{\mathrm{xb}} \int_{-\infty}^{\infty} x \frac{dn_{\mathrm{ss}}}{dx} e^{-t(f(x)+g(x))} dx. \tag{5}$$

This perturbation response may be rewritten as a sum of exponential relaxations with a strain-dependent relaxation time-constant $\tau(x)$ and strain-dependent ensemble stiffness $k(x)$ that is given by,

$$\Delta F(t) = a \int_{-\infty}^{\infty} k(x) e^{-t/\tau(x)} dx, \tag{6}$$

$$k(x) = -M\lambda_{\mathrm{xb}} x \frac{dn_{\mathrm{ss}}(x)}{dx}, \text{ and} \tag{7}$$

$$\tau(x) = \frac{1}{f(x) + g(x)}. \tag{8}$$

Therefore, the entire relaxation process may be thought of as being comprised of an infinity of exponentially relaxing sub-processes where the strain-dependent stiffness $k(x)$ is the weight and $\tau(x)$ the relaxation timescale for each sub-processes. To obtain a dynamic stiffness $K(\omega)$, we use the Laplace transforms of equation (6) and of the step length perturbation to arrive at

$$K(\omega) = \left| \int_{-\infty}^{\infty} k(x) \frac{i\omega}{i\omega + 1/\tau(x)} dx \right|. \tag{9}$$

The integrand is the mechanical impedance of a Maxwell body, a spring mechanically in series with a dashpot, and a mechanical analogy can thus be drawn between ensemble crossbridge dynamics and Maxwell bodies. We demonstrate the analogy for the two-state model using Huxley's choices for the rate functions $f(x)$ and $g(x)$ (Huxley, 1957, figure 4b) given as

$$f(x) = \begin{cases} f_1 x \text{ for } 0 \leq x \leq h, \\ 0 \text{ otherwise,} \end{cases} \quad \text{and} \tag{10}$$

$$g(x) = \begin{cases} g_2 \text{ for } x < 0, \\ g_1 x \text{ for } x \geq 0. \end{cases} \tag{11}$$

which leads to the steady-state bond distribution $n_{\mathrm{ss}}(x)$

$$n_{\mathrm{ss}} = \begin{cases} f_1/(f_1 + g_1) \text{ for } 0 < x \leq h \\ 0 \text{ otherwise.} \end{cases} \tag{12}$$

Applying equations (7 – 9), the dynamic stiffness corresponding to Huxley's choices of $f(x)$ and $g(x)$ is that of a single Maxwell body with stiffness $k(h)$ and damping coefficient $b = k(h)/(f(h)+g(h)) = k(h)\tau(h)$. To add more detail, the rectangular waveform of the steady-state bond distribution [equation (12)] implies that $k(x)$ of equation (7) is a sum of two δ-functions, a negative one at $x = 0$ and a positive one at $x = h$. However, because the delta

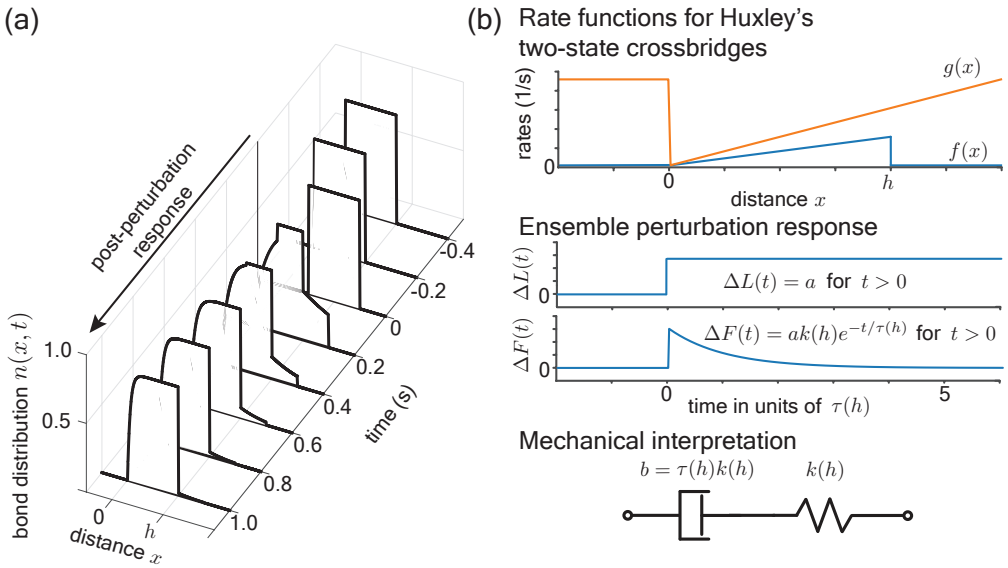

Figure 4: The rheology of an ensemble of Huxley's two-state crossbridges. (a) The time-evolution of the bond distribution in response to a step length perturbation. (b) Rheology of an ensemble of Huxley's two-state crossbridges. The ensemble's perturbation response exponentially relax with time-constant $\tau(h) = 1/(f(h) + g(h))$ where $f(x)$ and $g(x)$ are the rate functions and h is the powerstroke distance. A mechanical interpretation of this single exponential relaxation is of a spring in series with a dashpot.

at $x = 0$ does not contribute to the perturbation response, only the delta at $x = h$ remains and the overall perturbation response is that of a single Maxwell body. Huxley's choices thus lead to an exact correspondence between ensemble crossbridge dynamics and a single Maxwell body, which justifies the mechanical interpretation for the high and low frequency rheological behaviors observed in figure 3 as elastic and viscous behaviors. The spring-like behavior at high frequencies is not surprising because springs are built into ensemble crossbridge models by idealizing each crossbridge as an individual spring, all of which adds up at high frequencies. On the other hand, there are no dampers built into crossbridge models and the low-frequency behavior thus arise as an emergent property of the ensemble rather than as an intrinsic property of crossbridges. Specifically, each crossbridge dissipate stored elastic energy as they cycle and this dissipation averaged over the entire ensemble and over many cycles manifests as an effective damping coefficient at low frequencies.

As shown, $k(x)$ of equation (7) is well-approximated by a δ-function for Huxley's two-state model leading to single exponentially relaxing sub-process that dominates the entire perturbation response. Thus whether we need the full ensemble model or if we can approximate the response with just a few discrete relaxation sub-processes depends on whether $k(x)$ shows localizations in x or not. We hypothesize that, for all crossbridge models considered in this paper, the localization is a dominant feature and that only a few discrete relaxation sub-processes are needed to capture the emergent rheological features on intermediate frequencies [figure 3b]. Because $k(x)$ is proportional to the derivative of the steady-state bond distribution, its localization and the resulting exponential sub-process directly equate to either a sharp rising or falling edge of the steady-state bond distribution, or of multiple

bond distributions for crossbridge models with multiple attached states. We shall verify the hypothesis by fitting exponential sub-processes to the dynamic stiffness computed for the crossbridge models and examine if those fitted processes corresponds to rising or falling edges of the bond distribution.

Low-order models of multi-state crossbridge ensembles

Crossbridge dynamics are generally more complex than Huxley's two-state model and may have multiple internal states that introduce higher-order dynamics. Nevertheless, the perturbation force response initially arises from stretching bound crossbridges and its long-term relaxation is because of a redistribution of the crossbridges between the various possible states. This suggests an approach to tackle the behavior in the intermediate frequencies where crossbridge models were shown to deviate from the simple asymptotic behavior of a Maxwell body (figure 3b). Namely that, under more complicated attachment-detachment dynamics, the perturbation response would show multiple exponential relaxation sub-processes. So we investigate whether a finite number of exponential relaxations can capture the emergent ensemble rheologies in spite of possible complexities, under the hypothesis that a few sub-processes dominate the response.

We find that at most three exponentially relaxing sub-processes accurately capture the frequency-dependent stiffness over seven orders of magnitude on the frequency axis [figure 5a, Methods B, Figure 5 - Table Supplement 1]. Huxley's two state model fit exactly with a single relaxation, consistent with our earlier derivation. The five-state model appears to be a close fit to two sub-processes. The three- and four-state models are mostly fitted by three relaxations although there are identifiable differences. Our fitting procedure using four and five exponential relaxations did not generate appreciable better fits and implies that these crossbridge models incorporate dynamics that cannot be easily distinguished without a large number of exponential relaxations. Overall, the accurate fits demonstrates that, although crossbridge models incorporate a vast parameter space, the rheologies exhibited by their ensemble dynamics are far simpler and dominated by only a few exponentially relaxing sub-processes.

The fitting process is a general procedure able to find sub-processes acting on vastly different timescales and has been applied to the measured rheology of muscles to identify the dominant sub-processes (Kawai and Brandt, 1980; Kawai et al., 1993), but how to connect the fitted values to the cycling of crossbridges remains an open question. We use the three-state model (Murase et al., 1986) as a test case to examine the connection suggested by our analysis of Huxley's two-state model. The three-state model exhibits a significant dip in the dynamic stiffness that is indicative of a negative exponential sub-process that has been attributed to a delayed tension rise observed in a muscle's perturbation response (Kawai et al., 2021). The three-state model has two attached states with steady-state distributions $n_{1,\mathrm{ss}}(x)$ and $n_{2,\mathrm{ss}}(x)$ and governed by the kinetic scheme illustrated in [figure 5b]. Our earlier analysis with equation (7) suggests that the derivatives of these distributions drive the perturbation response and that local peaks would identify the dominant sub-processes of the three-state model [figure 5c]. Namely, we examine $\lambda_1 x dn_{1,\mathrm{ss}}(x)/dx$ and $\lambda_2 x dn_{2,\mathrm{ss}}(x)/dx$ where λ_1 and λ_2 are crossbridge stiffnesses for the first and second attached states, respectively. We find that matching the peaks of these two curves identifies the fitted time-constants [Figure 5 -

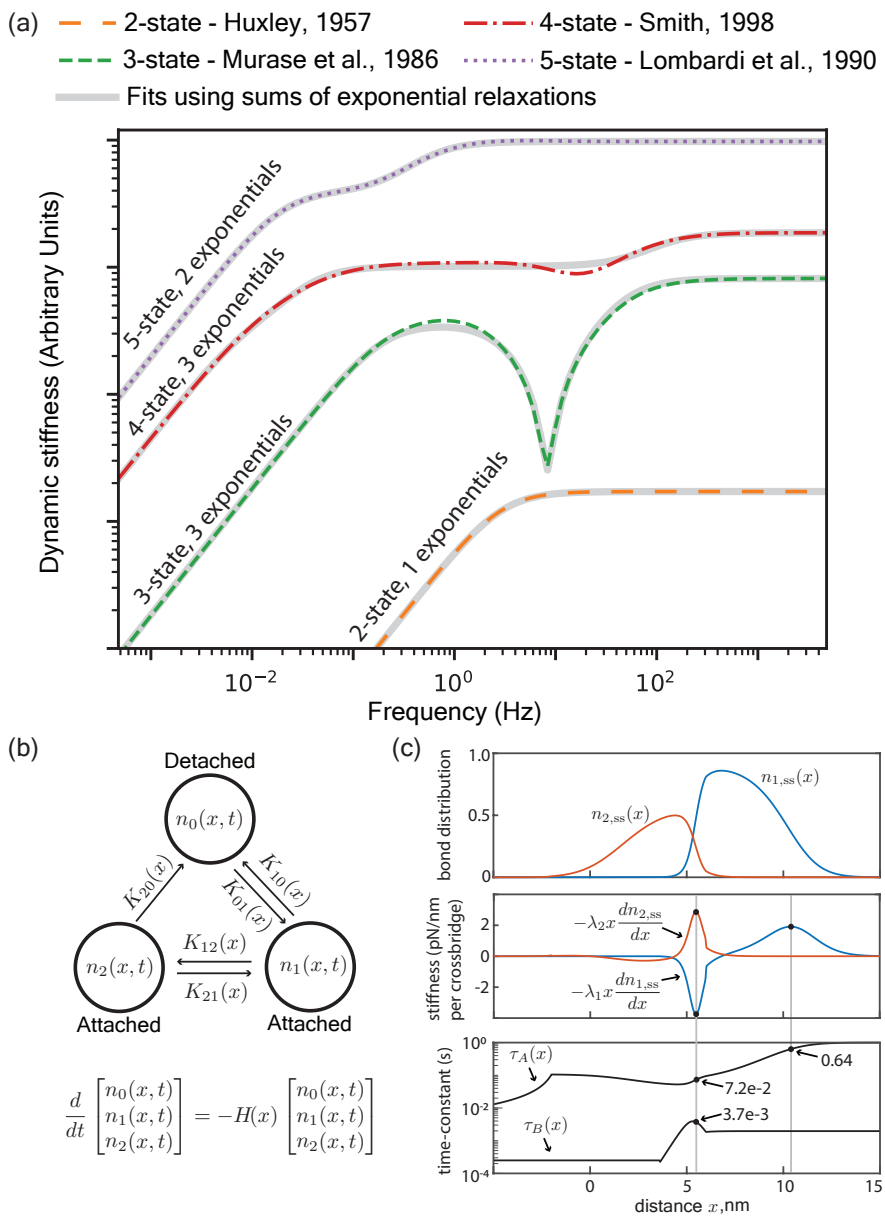

Figure 5: (a) The dynamic stiffness of different crosssbridge ensembles are accurately fitted by at most 3 time-constants, each associated with an exponential process [See Figure 5 - Table Supplement 1 for fitted values]. The traces are vertically shifted for clarity [see Figure 3 - Figure Supplement 1 for an unmodified plot]. (b) Kinetic scheme of a three-state crossbridge model (Murase et al., 1986). The matrix $H(x)$ is a state transition matrix with two non-zero eigenvalues $1/\tau_A$ and $1/\tau_B$. (c) Examination of the derivatives of the steady-state distributions shows that the local peaks accurately identifies the time-constants fitted in Figure 5 - Table Supplement 1.

Table Supplement 2] within a 15% error, which is remarkably accurate considering that the fitting process parsed frequencies spanning seven orders of magnitude. This suggests that the fitted sub-processes are measuring these local peaks in the derivative of the steady-state

distributions, which correspond to the rising and falling edges of steady-state distributions [figure 5c]. To be more precise, the curves to examine should be two separate linear combinations of $\lambda_1 x dn_{1,\mathrm{ss}}(x)/dx$ and $\lambda_2 x dn_{2,\mathrm{ss}}(x)/dx$ rather than each independently but our more detailed analysis show nearly identical results [Methods C].

Our examination of multi-state crossbridge models puts forth the following connection between the exponential relaxation fitted to muscle rheology and the dynamics of crossbridge cycling. Namely, each fitted relaxation results from either a sharp rising or falling edge of the steady-state bond distribution of attached crossbridge states. Assuming that most crossbridges attach at positive x, the fitted stiffness is positive for a falling edge and negative for a rising edge. The fitted time-constant are associated with the attachment and detachment rates corresponding to the rising or falling edges of the steady-state bond distributions. Furthermore, because the forces arising from the edges are modulated by x, the falling edge at larger x can dominate over the rising edge at smaller x, such as in the case of Huxley's two-state model. Therefore, although the bond distributions themselves may be of a complicated functional form due to the vast parameter space that multi-state crossbridge models tend to require, the emergent ensemble rheology is simpler and dominated by few rising and falling edges. This simplification affords a parameter reduction of multi-state crossbridge models down to two per exponential relaxation, a stiffness and a time-constant, and will allow us to compute the rheological behavior of ensemble crossbridge models in large-scale musculoskeletal simulations in a manner as efficient as phenomenological Hill-type muscle models but without compromising on the mechanistic, crossbridge-based understanding.

Discussion

Much like Zahalak's distribution-moment formalism (Zahalak, 1981), our results simplify the complexity of crossbridge models and connect vastly different scales. But we go further and analyze how modeling choices of a single crossbridge cycle give rise to macroscopically measurable quantities, a muscle's bulk rheological characterization. We focused on the dynamic stiffness which generalizes upon notions of elastic stiffness and viscous damping as a viscoelastic property that depend on the time-duration of interest. We showed with numerical computations that the emergent rheology of crossbridge ensembles can be accurately fitted by only a few exponential relaxation processes, without the need for simplifying assumptions about the underlying crossbridge model. The fitting procedure can and has been applied to empirical muscle data to identify the dominant exponential relaxations (Kawai and Brandt, 1980; Kawai et al., 1993), and we show that these relaxation corresponds to either a rising or falling edge in the steady-state bond distributions.

Exponential relaxations have long been used as phenomenological models of muscle rheology. Fading memory models of cardiac studies (Hunter et al., 1998) and Kawai and Brandt models (Kawai and Brandt, 1980; Kawai et al., 1993) are all sums of exponential relaxations. We showed here that exponential relaxations also arise from the rheology of crossbridge ensembles, and therefore are a common element connecting the microscopic with macroscopic models of muscle. When designing crossbridge models, the modeling choices however complex must map to the exponential relaxations observed in experiments for which three or four are found to accurately capture a muscle's rheology depending the muscle type (Kawai

and Brandt, 1980; Kawai et al., 1993). Each exponential adds two parameters, a stiffness and a time-constant, so at most eight parameters are justified from length perturbation experiments alone and any additional parameters must be estimated from other experiments. The additional parameters affect forces not included in the linear rheology, namely, nonlinear rheological features and the active contractile forces that operate in parallel to the rheology. On the other hand, when modeling the perturbation response of muscle, exponentials will do as well as detailed crossbridge models but remain grounded to crossbridge theory. Furthermore, using exponentials to compute a perturbation response for any small-amplitude length perturbation can be solved several orders of magnitude faster than directly solving the PDEs of crossbridge models. This computation efficiency affords large-scale biomechanical simulations in real-time, a principal reason why Hill-type muscle models are preferred over detailed crossbridge models in spite of their shortcomings (De Groote and Falisse, 2021; O'Neill et al., 2013; Miller, 2014).

We use the fact that exponential relaxations underlie the ensemble crossbridge dynamics to identify the limits of crossbridge theory in capturing muscle rheology. One limitation is that exponential relaxations have a finite memory determined by its time-constant, so an ensemble of crossbridges cannot remember its perturbation history far beyond its longest time-constant. Residual force enhancement and force depression are history-dependent phenomena that have implications for the motor control of muscles (Herzog, 2004), and are in clear contradiction with having an exponentially decaying memory. In these phenomena, the forces exhibited by a muscle fiber upon being stretched or shortened to a final length relax towards a value that is persistently higher (force enhancement) or lower (force depression) than if the muscle fiber were isometrically held at the final length. So although forces relax, the muscle fiber always have a memory of being stretched or shortened, unlike exponentials, which supports the current understanding that history-dependent muscle phenomena lie outside the purview of current crossbridge models. However, such history-dependence parallels phenomena found in other biological and non-biological materials for which an empirically derived fractional viscoelasticity aptly captures their perturbation response that relax as a power-law rather than an exponential (Jaishankar and McKinley, 2013; Bagley and Torvik, 1983; Kollmannsberger and Fabry, 2011). Drawing analogies between muscles and these fractional viscoelastic materials may help to better understand the physical underpinnings of residual force enhancement and depression in muscles.

A second limitation is the neural control of a muscle's perturbation response. Consider a muscle's perturbation response modeled as a single exponential relaxation with coefficient k and time-constant τ that now depend on a neural input u. We argued previously that a requirement on τ is that it increases with neural input u or intracellular calcium concentration (Nguyen et al., 2018). This is to ensure that the same muscle can be used as an elastic structure when highly activated and as a viscous structure when weakly activated. We find that the time-constants arising from crossbridge ensembles do not follow this trend. In the simplest implementation of neural control, the number of crossbridges in an ensemble increases with calcium concentration. However, more crossbridges would increase coefficient k but leave τ unchanged because crossbridge cycling is unaffected. Some crossbridge models incorporate faster crossbridge cycling with higher calcium (Zahalak, 1986; Zahalak and Ma, 1990; Walcott, 2014). While this leads to higher contractile forces, the time-constant would decrease with higher calcium rather than increase. These arguments may be seen in equations

(7 - 8) for a two-state crossbridge model in which the time-constant does not depend on crossbridge density M and decreases with higher values of attachment f or detachment g.

The mismatches between exponential relaxations, known muscle phenomena, and requirements of neural control all suggest that either crossbridge models currently lack an essential feature or that non-crossbridge elements come into play. There are multiple possible candidate resolutions that we speculate on, may operate in unison, and certainly require further experimental studies. Thick and thin filament compliance between neighboring crossbridges can store elastic energy that dissipate far slower than the crossbridges themselves and affect muscle forces on long experimental timescales (Mijailovich et al., 1996; Daniel et al., 1998). Intersarcomeric dynamics may lead to dynamics not captured by single sarcomere model such that the number of participating sarcomeres can drastically alter the rheology of a muscle fiber (Shimamoto et al., 2009; Campbell, 2009). Titin can directly modulate force transmission across a sarcomere and therefore may affect crossbridge dynamics (Nishikawa et al., 2012; Powers et al., 2014). Neural feedback could enforce time-constants as needed depending on motor tasks but is limited by transmission delays on the order of 50ms for humans (Johansson and Cole, 1994; Hogan et al., 1987). All of these possibilities require further research and analysis, but point to a shortcoming in the current crossbridge theory for muscle forces and rheology.

Conclusions

In this paper, we analyze the microscopic models of muscle forces to identify a minimal parameter-set that captures the bulk rheological properties of muscle and to provide a mechanistic interpretation of these bulk properties in terms of the microscopic models. Specifically, we performed numerical simulations of ensemble crossbridge models of varying complexities to find a common rheology at asymptotically high and low frequencies. An in-depth analysis into the simplest two-state crossbridge model suggests that the common rheological element is an exponential relaxation of forces, which has a mechanical interpretation as a Maxwell body, i.e. a spring and damper in series. We find that crossbridge models differ only in the number of exponential relaxations and that we need at most three to accurately capture their rheologies. So although crossbridge models are complex, their rheologies are more tractable in terms of fewer parameters and lesser computational burden. Exponential relaxations have long been used as phenomenological fits to muscle rheology and our results show how they can be interpreted in terms of the underlying crossbridges dynamics. Thus, this decomposition into exponential relaxations is grounded to crossbridge dynamics yet provides new perspectives into muscle rheology that previously were clouded by the complexity of crossbridge models.

Author Contributions: K.D.N. and M.V. conceived the research, designed the research, analyzed and interpreted the results, and wrote the paper.

Competing interests: The authors declare no competing interests.

Methods

A Dynamic stiffness calculation of crossbridge models

We detail here the numerical calculation of dynamic stiffness for ensemble crossbridge models. Although each model differs in number of internal states, a general differential equation for the mass balance between states can be written. Let j be the index for the states, then $n_j(x,t)$ is the distribution of crossbridges in the jth state at time t and with distance x to the nearest binding site. The mass balance will take the general form

$$\frac{dn_j(x,t)}{dt} = P_j(x, n_1(x,t), n_2(x,t), ..., N_1(t), N_2(t), ...) \tag{13}$$

where $N_j(t) = \int_{-\infty}^{\infty} n_j(x,t)dx$ is the total proportion of crossbridges in state j and P_j is a function that depends on the crossbridge model. We use P_j as given by four different models varying from two to five internal states (Huxley, 1957; Smith, 1998; Murase et al., 1986; Lombardi and Piazzesi, 1990).

We impose a step length perturbation of amplitude a and use the output force perturbation response to numerically compute each model's dynamic stiffness. Specifically, we numerically integrate equation (13) subjected to the initial condition $n_j(x,0) = n_{j,\text{ss}}(x-a)$ using the explicit fourth-order Runge-Kutta (RK4) scheme (Press et al., 2007). The integration takes time steps of size δt and terminates at a finite time T. The output force perturbation response is a discrete time series ΔF_m indexed in time by m and calculated as

$$\Delta F_m = \sum_j \int_{-\infty}^{\infty} k_j(x - x_{0,j})(n_j(x, m\delta t) - n_{j,\text{ss}}(x))dx \tag{14}$$

for stiffness k_j and neutral length $x_{0,j}$ that depends on the jth crossbridge state. The dynamic stiffness $K(\omega)$ is then computed in terms of z-transforms as

$$K(\omega) = \left| \frac{\sum_m \Delta F_m z^{-m}}{\sum_m \Delta L_m z^{-m}} \right|_{z=\exp(-i\omega\delta t)} \tag{15}$$

where ΔL_m is the step length perturbation equal to a for all $m \geq 0$ and zero otherwise.

To calculate the dynamic stiffness for Huxley's two-state model (Huxley, 1957) in dimensional units, we use parameter values $(f_1, g_1, g_2) = (15, 4, 85)s^{-1}$ provided by (Zahalak and Ma, 1990) (Zahalak and Ma, 1990). We also used a crossbridge stiffness $k_{\text{xb}} = 0.5\text{pN/nm}$ that is consistent with literature values (Lombardi and Piazzesi, 1990; Smith, 1998).

B Fitting procedure

We detail here the process of fitting exponential relaxations to the dynamic stiffness of different crossbridge models [figure 3d]. We denote ω_j as the frequency indexed by j and logarithmically sampled from $5 * 10^{-4}$ Hz to $5 * 10^3$Hz. We also denote $K(\omega_j)$ as the numerically determined dynamic stiffness at frequency ω_j. The objective is to find N-pairs of

parameters (k_m, τ_m) indexed by m such that the function

$$y(\omega_j) = \left| \sum_{m=1}^{N} k_m \frac{i\omega_j \tau_m}{1 + i\omega_j \tau_m} \right| \tag{16}$$

accurately captures $K(\omega_j)$ where N is the number of exponential relaxations to fit and i is the imaginary number. We defined fit to be the N-pairs of parameters (k_m, τ_m) that minimizes the cost

$$\sum_j (log(y(\omega_j)) - log(K(\omega_j)))^2 \tag{17}$$

where we use the log function to equally weight behaviors at vastly different frequencies. The fit was performed starting at $N = 1$ and N is incrementally increased until there is no appreciable difference between the fits at N and at $N + 1$.

All optimization procedures are performed using the Python 'scipy.optimize' library (Virtanen et al., 2020).

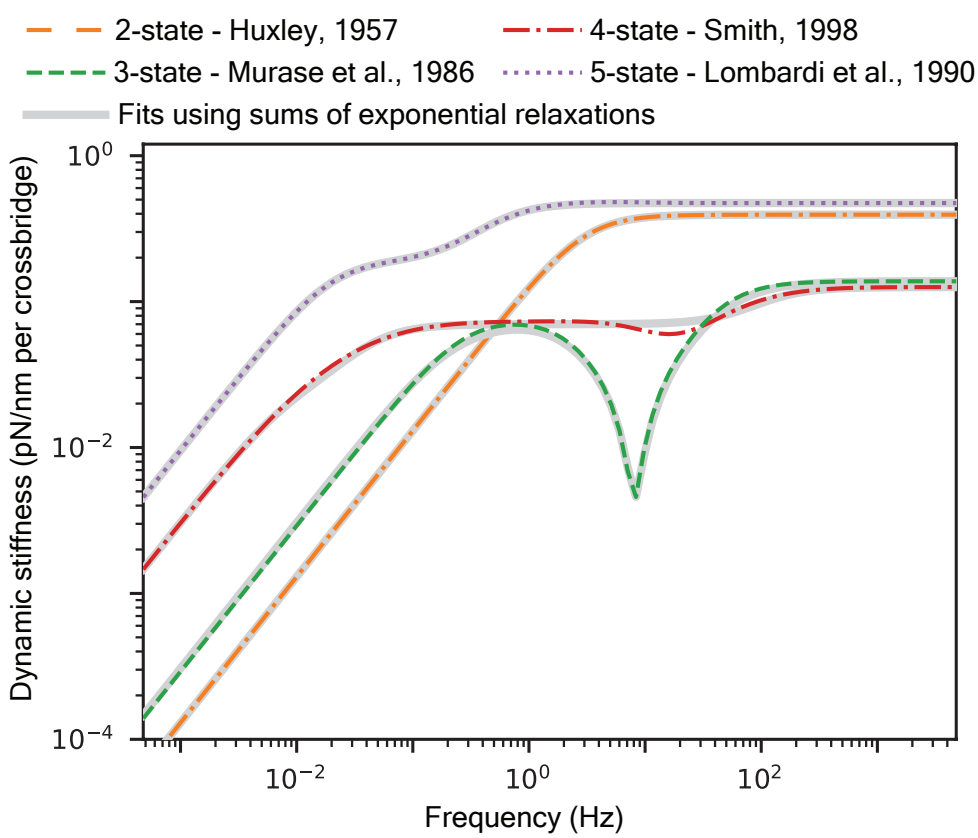

Figure 3 - Figure Supplement 1: Fitted curves to the dynamic stiffness of different crossbridge models.

C Perturbation analysis of three-state crossbridge model

We expand here the generalized two-state analysis to the three-state model by Murase et al., 1986 to identify the dominant time-constants in the system and compare them with the fitted

Model	k_1	τ_1	k_2	τ_2	k_3	τ_3
Huxley, 1957	0.39	5.3e-2	-	-	-	-
Murase et al., 1986	0.09	0.59	-0.10	6.8e-2	0.15	3.2e-3
Smith, 1997	0.05	2.0	-0.12	3.6	0.20	1.4e-3
Lombardi et al., 1990	0.18	8.0	0.30	0.28	-	-

Table Figure 5 - Table Supplement 1: Fitted parameters for figure 5a. Stiffness values are in units of pN/nm per crossbridge and time-constants are in units of seconds.

Model	Fitted time-constants	Search using $xdn_{\text{ss}}(x)/dx$
Huxley, 1957	5.3e-2 seconds	5.3e-2 seconds
Murase et al., 1986	(0.59 , 6.8e-2 , 3.2e-3) seconds	(0.64 , 7.2e-2 , 3.7e-3) seconds

Table Figure 5 - Table Supplement 2: Comparison of fitted time-constants and time-constants identified by using local peaks in the derivatives of steady-state bond distributions for a two-state and a three-state crossbridge model. The peak of xdn_{ss}/dx for the two-state model [equation (11)] is computed exactly with a time-constant $\tau = 1/(f_1h + g_1h) = 5.3e-2$ seconds.

values of Figure 5 - Table Supplement 1. In the three-state model, there are two attached states with bond distributions $n_1(x,t)$ and $n_2(x,t)$ and a detached state with distribution $n_0(x,t)$. By defining a column vector $\vec{n} = [n_0, n_1, n_2]^T$, the governing dynamics of the system is given by

$$\frac{d\vec{n}(x,t)}{dt} = -H(x)\vec{n}(x,t) \tag{18}$$

$$\text{such that} \quad n_0(x,t) + n_1(x,t) + n_2(x,t) = 1 \tag{19}$$

and where $H(x)$ is a 3x3 state transition matrix defined by the kinetic scheme of figure 5b. These equations uniquely define the steady-state bond distribution at equilibrium which we denote as $\vec{n}_{\text{ss}}(x)$. Specifically, the state transition matrix has three eigenvector-eigenvalue pairs $(\vec{v}_A(x), 1/\tau_A(x))$, $(\vec{v}_B(x), 1/\tau_B(x))$, and $(\vec{n}_{\text{ss}}(x), 0)$ where τ_A and τ_B are the two time-constants driving the perturbation response and $\vec{v}_A(x)$ and $\vec{v}_B(x)$ are unit vectors.

Mirroring the generalized two-state derivation, the perturbation response to a step length of size a is obtained by setting $\vec{n}(x,0) = \vec{n}_{\text{ss}}(x-a)$ as the initial condition to arrive at

$$\vec{n}(x,t) = \vec{n}_{\text{ss}}(x) + e^{-H(x)t}(\vec{n}_{\text{ss}}(x-a) - \vec{n}_{\text{ss}}(x)) \tag{20}$$

$$= \vec{n}_{\text{ss}}(x) - ae^{-H(x)t}\frac{d\vec{n}_{\text{ss}}(x)}{dx} \tag{21}$$

where the second equality arises by restricting our attention to small perturbations. We now expand the matrix-vector multiplication on the RHS using eigendecomposition of $H(x)$ as

$$\vec{n}(x,t) - \vec{n}_{\text{ss}}(x) = -a\left(e^{-t/\tau_A(x)}w_A(x)\vec{\nu}_A(x) + e^{-t/\tau_B(x)}w_B(x)\vec{\nu}_B(x)\right) \tag{22}$$

where w_A and w_B are linear weights that satisfy the linear system

$$[\vec{\nu}_A(x), \vec{\nu}_B(x), \vec{n}_{\text{ss}}(x)] \begin{bmatrix} w_A(x) \\ w_B(x) \\ 0 \end{bmatrix} = \frac{d\vec{n}_{\text{ss}}(x)}{dx}. \tag{23}$$

The third linear weight is necessary zero because $(\vec{n}(x,t) - \vec{n}_{\text{ss}}(x))$ in equation (22) must decay to zero and cannot have a component parallel to $n_{\text{ss}}(x)$ which does not decay.

The perturbation response is the first moment of equation (22) multiplied by a stiffness vector that maps the bond distributions to forces. It is given in terms of crossbridge density M, stiffness of the first attached state λ_1, and stiffness of the second attached state λ_2 as

$$\Delta F(t) = a \int_{-\infty}^{\infty} \left[k_A(x) e^{-t/\tau_A(x)} + k_B(x) e^{-t/\tau_B(x)} \right] dx \tag{24}$$

$$\text{where} \quad k_A(x) = -Mxw_A(x) \langle [0, \lambda_1, \lambda_2]^T, \vec{\nu}_A(x) \rangle \tag{25}$$

$$\text{and} \quad k_B(x) = -Mxw_B(x) \langle [0, \lambda_1, \lambda_2]^T, \vec{\nu}_B(x) \rangle. \tag{26}$$

The operator $\langle \cdot \rangle$ denotes the dot product between two column vectors. The first entry in the stiffness vector is set to zero to represent the detached crossbridge state. Our analysis of the generalized two-state crossbridge model suggests that dominant time-constants appears where either $k_A(x)$ or $k_B(x)$ are localized, and we find that these time-constants do not significantly differ from heuristically using the derivatives of the steady-state distributions [figure 5 - Figure Supplement 1].

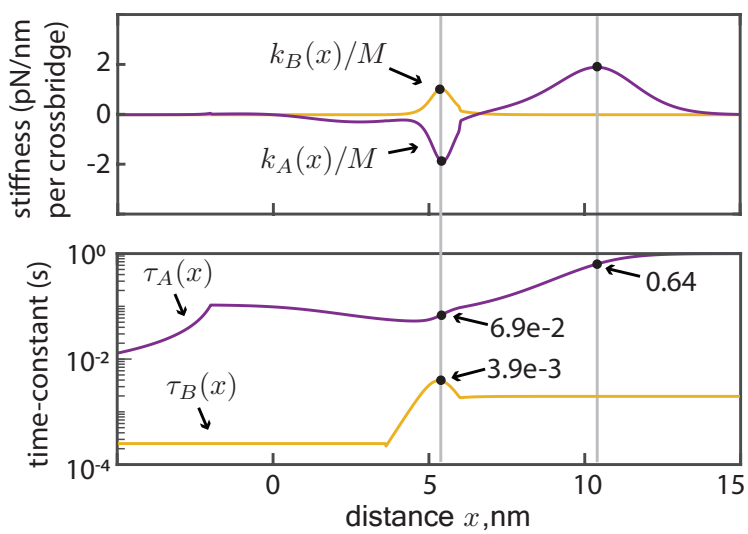

Figure 5 - Figure Supplement 1: Examination of the local peaks in stiffnesses $k_A(x)$ and $k_B(x)$ identifies the dominant time-constants. The stiffnesses are computed using an eigenvector analysis of the state-transition matrix $H(x)$ and are different from $\lambda_1 x dn_{1,\text{ss}}(x)/dx$ and $\lambda_2 x dn_{2,\text{ss}}(x)/dx$ used in figure 5c as a heuristic search. The identified time-constants do not significantly differ from the values found in figure 5c.

References

Bagley, R. L. and Torvik, P. (1983). A theoretical basis for the application of fractional calculus to viscoelasticity. *Journal of Rheology* **27**, 201–210.

Biewener, A. A. and Roberts, T. J. (2000). Muscle and tendon contributions to force, work, and elastic energy savings: a comparative perspective. *Exercise and Sport Sciences Reviews* **28**, 99–107.

Bizzi, E., Chapple, W. and Hogan, N. (1982). Mechanical properties of muscles: Implications for motor control. *Trends in Neurosciences* **5**, 395–398.

Campbell, K. S. (2009). Interactions between connected half-sarcomeres produce emergent mechanical behavior in a mathematical model of muscle. *PLoS Computational Biology* **5**, e1000560.

Cole, G. K., van den Bogert, A. J., Herzog, W. and Gerritsen, K. G. (1996). Modelling of force production in skeletal muscle undergoing stretch. *Journal of Biomechanics* **29**, 1091–1104.

Daniel, T. L., Trimble, A. C. and Chase, P. B. (1998). Compliant realignment of binding sites in muscle: transient behavior and mechanical tuning. *Biophysical Journal* **74**, 1611–1621.

De Groote, F. and Falisse, A. (2021). Perspective on musculoskeletal modelling and predictive simulations of human movement to assess the neuromechanics of gait. *Proceedings of the Royal Society B* **288**, 20202432.

Dick, T. J., Biewener, A. A. and Wakeling, J. M. (2017). Comparison of human gastrocnemius forces predicted by hill-type muscle models and estimated from ultrasound images. *Journal of Experimental Biology* **220**, 1643–1653.

Fung, Y. (1971). Comparison of different models of the heart muscle. *Journal of Biomechanics* **4**, 289–295.

Fung, Y.-C. (2013). *Biomechanics: mechanical properties of living tissues*. Springer Science & Business Media.

Gardel, M., Shin, J. H., MacKintosh, F., Mahadevan, L., Matsudaira, P. and Weitz, D. A. (2004). Elastic behavior of cross-linked and bundled actin networks. *Science* **304**, 1301–1305.

Herzog, W. (2004). History dependence of skeletal muscle force production: implications for movement control. *Human movement science* **23**, 591–604.

Hill, A. V. (1938). The heat of shortening and the dynamic constants of muscle. *Proceedings of the Royal Society of London. Series B-Biological Sciences* **126**, 136–195.

Hogan, N., Bizzi, E., Mussa-Ivaldi, F. A. and Flash, T. (1987). Controlling multijoint motor behavior. *Exercise and Sport Sciences Reviews* **15**, 153–190.

Holmes, K. C. (1997). The swinging lever-arm hypothesis of muscle contraction. *Current Biology* **7**, R112–R118.

Hunter, P., McCulloch, A. and Ter Keurs, H. (1998). Modelling the mechanical properties of cardiac muscle. *Progress in Biophysics and Molecular Biology* **69**, 289–331.

Huxley, A. and Tideswell, S. (1996). Filament compliance and tension transients in muscle. *Journal of Muscle Research & Cell Motility* **17**, 507–511.

Huxley, A. F. (1957). Muscle structure and theories of contraction. *Prog. Biophys. Biophys. Chem* **7**, 255–318.

Huxley, A. F. and Simmons, R. M. (1971). Proposed mechanism of force generation in striated muscle. *Nature* **233**, 533–538.

Jaishankar, A. and McKinley, G. H. (2013). Power-law rheology in the bulk and at the interface: quasi-properties and fractional constitutive equations. *Proceedings of the Royal Society A: Mathematical, Physical and Engineering Sciences* **469**, 20120284.

Johansson, R. S. and Cole, K. J. (1994). Grasp stability during manipulative actions. *Canadian Journal of Physiology and Pharmacology* **72**, 511–524.

Kawai, M. and Brandt, P. W. (1980). Sinusoidal analysis: a high resolution method for correlating biochemical reactions with physiological processes in activated skeletal muscles of rabbit, frog and crayfish. *Journal of Muscle Research & Cell Motility* **1**, 279–303.

Kawai, M., Saeki, Y. and Zhao, Y. (1993). Crossbridge scheme and the kinetic constants of elementary steps deduced from chemically skinned papillary and trabecular muscles of the ferret. *Circulation Research* **73**, 35–50.

Kawai, M., Stehle, R., Pfitzer, G. and Iorga, B. (2021). Phosphate has dual roles in cross-bridge kinetics in rabbit psoas single myofibrils. *Journal of General Physiology* **153**.

Koenderink, G. H., Dogic, Z., Nakamura, F., Bendix, P. M., MacKintosh, F. C., Hartwig, J. H., Stossel, T. P. and Weitz, D. A. (2009). An active biopolymer network controlled by molecular motors. *Proceedings of the National Academy of Sciences* **106**, 15192–15197.

Kollmannsberger, P. and Fabry, B. (2011). Linear and nonlinear rheology of living cells. *Annual review of materials research* **41**, 75–97.

Konow, N., Azizi, E. and Roberts, T. J. (2012). Muscle power attenuation by tendon during energy dissipation. *Proceedings of the Royal Society B: Biological Sciences* **279**, 1108–1113.

Lee, S. S., Arnold, A. S., de Boef Miara, M., Biewener, A. A. and Wakeling, J. M. (2013). Accuracy of gastrocnemius muscles forces in walking and running goats predicted by one-element and two-element hill-type models. *Journal of Biomechanics* **46**, 2288–2295.

Lin, D. C. and Rymer, W. Z. (2000). Damping actions of the neuromuscular system with inertial loads: soleus muscle of the decerebrate cat. *Journal of Neurophysiology* **83**, 652–658.

Lindstedt, S. L., LaStayo, P. and Reich, T. (2001). When active muscles lengthen: properties and consequences of eccentric contractions. *Physiology* **16**, 256–261.

Liu, C., Kawana, M., Song, D., Ruppel, K. M. and Spudich, J. A. (2018). Controlling load-dependent kinetics of β-cardiac myosin at the single-molecule level. *Nature structural & molecular biology* **25**, 505–514.

Lombardi, V. and Piazzesi, G. (1990). The contractile response during steady lengthening of stimulated frog muscle fibres. *The Journal of Physiology* **431**, 141–171.

Lymn, R. and Taylor, E. W. (1971). Mechanism of adenosine triphosphate hydrolysis by actomyosin. *Biochemistry* **10**, 4617–4624.

MacIntosh, B. R. and MacNaughton, M. B. (2005). The length dependence of muscle active force: considerations for parallel elastic properties. *Journal of Applied Physiology* **98**, 1666–1673.

McNamara, J. W., Li, A., Dos Remedios, C. G. and Cooke, R. (2015). The role of super-relaxed myosin in skeletal and cardiac muscle. *Biophysical reviews* **7**, 5–14.

Mijailovich, S. M., Fredberg, J. J. and Butler, J. P. (1996). On the theory of muscle contraction: filament extensibility and the development of isometric force and stiffness. *Biophysical Journal* **71**, 1475–1484.

Miller, R. H. (2014). A comparison of muscle energy models for simulating human walking in three dimensions. *Journal of biomechanics* **47**, 1373–1381.

Murase, M., Tanaka, H., Nishiyama, K. and Shimizu, H. (1986). A three-state model for oscillation in muscle: sinusoidal analysis. *Journal of Muscle Research & Cell Motility* **7**, 2–10.

Nguyen, K. D., Sharma, N. and Venkadesan, M. (2018). Active viscoelasticity of sarcomeres. *Frontiers in Robotics and AI* .

Nguyen, K. D. and Venkadesan, M. (2021). Rheological basis of skeletal muscle work loops. *arXiv* [**cond-mat.soft**], 2005.07238.

Niederer, S. A., Campbell, K. S. and Campbell, S. G. (2019). A short history of the development of mathematical models of cardiac mechanics. *Journal of molecular and cellular cardiology* **127**, 11–19.

Nishikawa, K., Biewener, A. A., Aerts, P., Ahn, A. N., Chiel, H. J., Daley, M. A., Daniel, T. L., Full, R. J., Hale, M. E., Hedrick, T. L. et al. (2007). Neuromechanics: an integrative approach for understanding motor control. *Integrative and Comparative Biology* **47**, 16–54.

Nishikawa, K. C., Monroy, J. A. and Tahir, U. (2018). Muscle function from organisms to molecules. *Integrative and Comparative Biology* **58**, 194–206.

Nishikawa, K. C., Monroy, J. A., Uyeno, T. E., Yeo, S. H., Pai, D. K. and Lindstedt, S. L. (2012). Is titin a 'winding filament'? a new twist on muscle contraction. *Proceedings of the royal society B: Biological sciences* **279**, 981–990.

Ogata, K. (2004). *System dynamics*, volume 13. Pearson/Prentice Hall Upper Saddle River, NJ.

O'Neill, M. C., Lee, L.-F., Larson, S. G., Demes, B., Stern, J. T. and Umberger, B. R. (2013). A three-dimensional musculoskeletal model of the chimpanzee (pan troglodytes) pelvis and hind limb. *Journal of Experimental Biology* **216**, 3709–3723.

Palmer, B. M. (2010). *A Strain-Dependency of Myosin Off-Rate Must Be Sensitive to Frequency to Predict the B-Process of Sinusoidal Analysis*, pp. 57–75. New York, NY: Springer New York.

Palmer, B. M., Swank, D. M., Miller, M. S., Tanner, B. C., Meyer, M. and LeWinter, M. M. (2020). Enhancing diastolic function by strain-dependent detachment of cardiac myosin crossbridges. *Journal of General Physiology* **152**.

Perreault, E. J., Heckman, C. J. and Sandercock, T. G. (2003). Hill muscle model errors during movement are greatest within the physiologically relevant range of motor unit firing rates. *Journal of Biomechanics* **36**, 211–8.

Powers, K., Schappacher-Tilp, G., Jinha, A., Leonard, T., Nishikawa, K. and Herzog, W. (2014). Titin force is enhanced in actively stretched skeletal muscle. *Journal of Experimental Biology* **217**, 3629–3636.

Press, W. H., William, H., Teukolsky, S. A., Saul, A., Vetterling, W. T. and Flannery, B. P. (2007). *Numerical recipes 3rd edition: The art of scientific computing.* Cambridge University Press.

Rack, P. M. and Westbury, D. (1974). The short range stiffness of active mammalian muscle and its effect on mechanical properties. *The Journal of Physiology* **240**, 331–350.

Rice, N., Jeong, S. and Nishikawa, K. (2020). How do muscle length and activation interact to determine muscle force production? In *Integrative and Comparative Biology*, volume 60, pp. E195–E195. Oxford University Press.

Sandercock, T. G. and Heckman, C. (1997). Force from cat soleus muscle during imposed locomotor-like movements: experimental data versus hill-type model predictions. *Journal of Neurophysiology* **77**, 1538–1552.

Shimamoto, Y., Suzuki, M., Mikhailenko, S. V., Yasuda, K. and Ishiwata, S. (2009). Inter-sarcomere coordination in muscle revealed through individual sarcomere response to quick stretch. *Proceedings of the National Academy of Sciences* **106**, 11954–11959.

Sleboda, D. A. and Roberts, T. J. (2020). Internal fluid pressure influences muscle contractile force. *Proceedings of the National Academy of Sciences* **117**, 1772–1778.

Smith, D. (1998). A strain-dependent ratchet model for [phosphate]-and [atp]-dependent muscle contraction. *Journal of Muscle Research & Cell Motility* **19**, 189–211.

Stewart, M. A., Franks-Skiba, K., Chen, S. and Cooke, R. (2010). Myosin atp turnover rate is a mechanism involved in thermogenesis in resting skeletal muscle fibers. *Proceedings of the National Academy of Sciences* **107**, 430–435.

Todorov, E. (2003). On the role of primary motor cortex in arm movement control. *Progress in Motor Control III* **6**, 125–166.

Tschoegl, N. W. (2012). *The phenomenological theory of linear viscoelastic behavior: an introduction*. Springer Science & Business Media.

van den Bogert, A., Gerritsen, K. and Cole, G. (1998). Human muscle modelling from a user's perspective. *Journal of Electromyography and Kinesiology* **8**, 119–124.

Virtanen, P., Gommers, R., Oliphant, T. E., Haberland, M., Reddy, T., Cournapeau, D., Burovski, E., Peterson, P., Weckesser, W., Bright, J. et al. (2020). SciPy 1.0: Fundamental Algorithms for Scientific Computing in Python. *Nature Methods* **17**, 261–272.

Walcott, S. (2014). Muscle activation described with a differential equation model for large ensembles of locally coupled molecular motors. *Physical Review E* **90**, 042717.

Weitz, D., Wyss, H. and Larsen, R. (2007). Oscillatory rheology: Measuring the viscoelastic behaviour of soft materials. *GIT Laboratory Journal Europe* **11**, 68–70.

Williams, C. D., Regnier, M. and Daniel, T. L. (2012). Elastic energy storage and radial forces in the myofilament lattice depend on sarcomere length. *PLoS computational biology* **8**, e1002770.

Zahalak, G. I. (1981). A distribution-moment approximation for kinetic theories of muscular contraction. *Mathematical Biosciences* **55**, 89–114.

Zahalak, G. I. (1986). A Comparison of the Mechanical Behavior of the Cat Soleus Muscle With a Distribution-Moment Model. *Journal of Biomechanical Engineering* **108**, 131–140.

Zahalak, G. I. and Ma, S.-P. (1990). Muscle activation and contraction: constitutive relations based directly on cross-bridge kinetics. *Journal of Biomechanical Engineering* **112**, 52–62.

Zajac, F. E. (1989). Muscle and tendon: properties, models, scaling, and application to biomechanics and motor control. *Critical Reviews in Biomedical Engineering* **17**, 359–411.